Search for H $\rightarrow WW^*$ Production with Matrix Element Methods at Tevatron Using 1.9 fb^{-1} Data

Text for the public web page – CDF note 8958

The CDF Collaboration
URL http://www-cdf.fnal.gov
(Dated: August 17, 2007)

We report a search for Standard Model Higgs to WW^* production in two charged lepton (e,μ) and two neutrino final state in $p\overline{p}$ collisions at $\sqrt{s} = 1.96$ TeV. The data were collected with the CDF II detector at the Tevatron collider at Fermilab and correspond to an integrated luminosity of 1.9 fb^{-1}. The Matrix Element method is used to calculate the event probability and construct a likelihood ratio discriminator. We find 522 candidates with an expectation of 513±41 background and 7.8±0.6 signal for Higgs mass 160GeV/c^2 at next-to-next-to-leading logarithmic level calculation. The observed 95% C.L. limit is 0.8 pb which is 2.0 times the Standard Model prediction while the median of expected limit is $3.1^{+1.3}_{-0.9}$ with systematics included. Results for 9 other Higgs mass hypotheses ranging from 110GeV/c^2 to 200GeV/c^2 are also presented.

PACS numbers:

I. INTRODUCTION

The Higgs boson is introduced into Standard Model through Higgs Mechanism to explain the electroweak symmetry breaking and the origins of particle mass. The current precision electroweak measurements tell us that the mass of the Standard-Model Higgs boson is lower than about 144 GeV/c^2 (one-sided 95 percent confidence level upper limit) and increases to 182 GeV/c^2 when including the LEP-2 direct search lower bound limit 114 GeV/c^2(95% CL limit)[1]. For this analysis we focus on gluon fusion production of Higgs through WW^* channel which is the dominant channel for $m_H > 135$ GeV/c^2[2]. The small production cross section, e.g. $\sigma_{NNLL}(H \to WW^*) = 0.388pb$ at m_H =160 GeV/c^2[3]), makes it challenging to be directly observed in hadron collider environment.

In this note, we present a search of $gg \to H \to WW^* \to l^+l^-\nu\bar{\nu}$, where $l^\pm$ = e, μ or τ with final states e^+e^-, $e^\pm\mu^\mp$ and $\mu^+\mu^-$. We use 1.1 fb^{-1} of integrated luminosity collected by the CDF II detector at the Fermilab Tevatron with collisions at $\sqrt{s} = 1.96$ TeV. The Matrix Element method is developed to calculate the event probability density for signal and background processes by using leading order matrix elements from MCFM[4] package.

The analysis strategy is to use a common event selection for 10 different Higgs mass hypotheses between 110GeV/c^2 to 200 GeV/c^2. For each Higgs mass point, an event-by-event likelihood ratio discriminator is constructed from event probability as a final observable.

II. DETECTOR DESCRIPTION

The components of the CDF II detector relevant to this analysis are described briefly here; a more complete description can be found elsewhere [5]. The detector geometry is described by the azimuthal angle ϕ and the pseudo-rapidity $\eta \equiv -\ln(\tan\theta/2)$, where θ is the polar angle of a particle with respect to the proton beam axis (positive z-axis). The pseudo-rapidity of a particle originating from the center of the detector is referred to as $\eta_{\rm det}$.

The trajectories of charged particles are reconstructed using silicon micro-strip detectors [6, 7] and a 96-layer open-cell drift chamber (COT) [8] embedded in a 1.4 T solenoidal magnetic field. For $|\eta_{\rm det}| \leq 1$, a particle traverses all 96 layers of the COT; this decreases to zero at $|\eta_{\rm det}| \approx 2$. The silicon system provides coverage with 6 (7) layers with radii between 2.4 cm and 28 cm for $|\eta_{\rm det}| < 1.0$ ($1.0 < |\eta_{\rm det}| < 2.0$). Outside of the solenoid are electromagnetic (EM) and hadronic (HAD) sampling calorimeters segmented in a projective tower geometry. The first hadronic interaction length (λ) of the calorimeter, corresponding to 19-21 radiation lengths (X_0), uses lead absorber for measuring the electromagnetic component of showers, while the section extending to 4.5-7 λ uses iron to contain the hadronic component. The calorimeters are divided in a central ($|\eta_{\rm det}| < 1$) and forward ($1.1 < |\eta_{\rm det}| < 3.64$) region. Shower maximum detectors (SMX) embedded in the electromagnetic calorimeters at approximately $6X_0$ help in the position measurement and background suppression for electrons. Outside of the central calorimeters are scintillators and drift chambers for identifying muons as minimum ionizing particles which are divided into central ($|\eta_{\rm det}| < 0.6$) and extended ($0.6 < |\eta_{\rm det}| < 1.0$) regions. We use three complementary track pattern recognition algorithms which are distinguished by their starting point in COT, silicon, or projection from calorimeter energy cluster to interaction region.

III. LEPTON IDENTIFICATION

In order to maximize signal acceptance and suppress backgrounds from jets and photons misidentified as leptons, we use two(four) categories of electrons(muons). A seventh category, based on central tracks that are not fiducial to calorimeters or muon detectors, is used as either an electron or muon in forming $H \to WW^*$ candidates. The resulting seven categories exploit essentially all the tracks and electromagnetic calorimeter clusters available.

All leptons are required to be isolated such that the sum of the E_T for the calorimeter towers in a cone of $\Delta R = \sqrt{(\Delta\eta)^2 + (\Delta\phi)^2} < 0.4$ around the lepton is less than 10% of the electron E_T or muon p_T. The transverse energy E_T of a shower or calorimeter tower is $E\sin\theta$, where E is the associated energy. Similarly, p_T is the component of track momentum transverse to the beam line.

Electron candidates are required to have a ratio of HAD energy to EM energy consistent with originating from an electromagnetic shower and are further divided into two central and two forward categories. Both central electron categories require a well-measured COT track satisfying $p_T > 10$ GeV/c which is fiducial to the central SMX and matched to a central EM energy cluster. The more stringent category additionally requires a matching cluster in the shower maximum detector, the energy sharing between towers to be small, and the ratio for shower energy E to track momentum p to be less than $2.5 + 0.0015E_T$. Forward electrons are required to be fiducial to the forward SMX detector and their energy deposition in both the calorimeter towers and SMX detector must be consistent with

an electron shower shape. One of the calorimeter seeded tracks need to be matched to a silicon track to reduce the photon background.

Muons are identified by either a charged track matched to a reconstructed track segment ("stub") in the central or extended muon chambers or as a stubless minimum ionizing particle fiducial to the central or forward calorimeter. All muons are required to deposit less than $2 + \max(0, 0.0115(p-100))$ GeV in the EM and $6 + \max(0, 0.028(p-100))$ GeV in the HAD calorimeters. In addition, stubless muons are required to have at least 0.1 GeV in total calorimeter energy. For $|\eta_{\rm det}| < 1.2$, strict requirements on the number of COT hits and the χ^2 of the track fit are placed on the muon tracks in order to suppress kaon decay-in-flight backgrounds. The category of stubless muons with $|\eta_{\rm det}| > 1.2$ requires that at least 60% of the COT layers crossed by the track have hits. In order to suppress background from cosmic rays, the track's point of closest approach to the beamline must be consistent with originating from the beam.

The final category of leptons are constructed from tracks which are not fiducial to the SMX detectors nor identified as stubbed muons. The requirements for the tracks are the same as stubless muons with $|\eta_{\rm det}| < 1.2$, but without any of the calorimeter requirements. Due to the lack of calorimeter information, electron and muons cannot be reliably differentiated in this region, and are therefore treated as having either flavor in the Higgs candidate selection. If an electron or non-fiducial track candidate is consistent with being due to a photon conversion as indicated by the presence of an additional nearby track, the candidate is vetoed.

To identify the presence of a Higgs boson decaying to two neutrinos, we use the missing transverse energy $\not\!\!E_T = |\sum_i E_{T,i}\ \hat{n}_{T,i}|$, where the $\hat{n}_{T,i}$ is the transverse component of the unit vector pointing from the interaction point to calorimeter tower i. The $\not\!\!E_T$ is corrected for muons which do not deposit all of their energy in the calorimeter.

The Higgs candidate events are required to pass one of four online trigger selections implemented in three successively more stringent levels. The final central electron requirement is an EM energy cluster with $E_T > 18$ GeV matched to a track with $p_T > 8$ GeV/c. Muon triggers are based on information from either of the two muon chambers matched to a track with $p_T > 18$ GeV/c. The fourth trigger which accepts forward electrons with an $E_T > 20$ GeV EM energy cluster and an online measurement of the $\not\!\!E_T > 15$ GeV[9].

IV. BASE SELECTION

We define a common Base selection for different Higgs mass observation. The $ll\nu\overline{\nu}$ candidates are selected from two opposite-sign leptons. At least one lepton is required to satisfy the trigger and have $E_T > 20$ GeV ($p_T > 20$ GeV/c) for electrons (muons). We loosen this requirement to > 10 GeV (GeV/c) for the other leptons to increase Higgs kinematic acceptance. The z-positions of all the leptons in a candidate at the point of closest approach to the beam-line are required to be within 4 cm of each other. The invariant mass of two leptons is required to be greater than 16 GeV/c^2.

There are several sources of background: Drell-Yan where the measured with large $\not\!\!E_T$ is due to resolution tails, $WZ \to lll\nu$ where one lepton is lost, $WW \to ll\nu\overline{\nu}$, $t\bar{t} \to b\bar{b}ll\nu\overline{\nu}$, and $W\gamma$ and W+jets where a photon or jet is misidentified as a lepton. Because of the significant backgrounds from $W\gamma$ and W+jets, we apply the addition isolation requirement on the leptons that the sum of the track p_T in a cone for $\Delta R < 0.4$ around each lepton is less than 10% if the electron E_T or muon p_T.

To suppress the Drell-Yan background, we require $\not\!\!E_{T\rm spec} > 25$ GeV, where $\not\!\!E_{T\rm spec}$ is defined to be:

$$\not\!\!E_{T\rm spec} \equiv \begin{cases} \not\!\!E_T & \text{if } \Delta\phi(\not\!\!E_T, \text{lepton, jet}) > \frac{\pi}{2} \\ \not\!\!E_T \sin(\Delta\phi(\not\!\!E_T, \text{lepton, jet})) & \text{if } \Delta\phi(\not\!\!E_T, \text{lepton, jet}) < \frac{\pi}{2} \end{cases}$$

This definition is a requirement that the $\vec{\not\!\!E}_T$ transverse to each lepton or jet in the event is at least 25 GeV if $\vec{\not\!\!E}_T$ points along that object, so that losing energy from just one such object in an event would not allow it to enter the sample. In order to suppress the effect of mis-measurement of the unclustered energy, we require that $\not\!\!E_{T,\rm sig} \equiv \not\!\!E_T/\sqrt{\sum E_T} > 2.5$ GeV$^{\frac{1}{2}}$, which is based on the fact that the calorimeter energy resolution is a approximately proportional to the square root of the total energy.

We further require the candidates to have less than 2 jets with $p_T > 15$ GeV and $|\eta| < 2.5$, in order to suppress $t\bar{t}$ backgrounds, $M_{\ell^+\ell^-} > 25$ GeV in order to suppress heavy flavor contributions, and exactly 2 leptons to suppress WZ contributions with a third lepton.

The expected and observed yields in the Base selection are shown in Table I and Table II

V. DATA MODELING

The geometric and kinematic acceptance for the WW, WZ, ZZ, $W\gamma$, W+jets, and $t\bar{t}$ processes are determined using a Monte Carlo calculation of the collision followed by a GEANT3-based simulation of the CDF II detector [10]

TABLE I: Expected and Observed Yields for Higgs at 10 different mass points in the Fit Region

	Higgs Mass (GeV)									
Category	110	120	130	140	150	160	170	180	190	200
$e\ e$	0.1	0.3	0.6	0.9	1.2	1.4	1.4	1.1	0.8	0.6
$e\ \mu$	0.2	0.6	1.3	2.0	2.6	3.1	3.0	2.5	1.8	1.4
$\mu\ \mu$	0.1	0.2	0.5	0.8	1.1	1.3	1.3	1.0	0.7	0.6
e trk	0.0	0.2	0.4	0.7	0.9	1.2	1.2	1.0	0.7	0.6
μ trk	0.0	0.1	0.2	0.4	0.6	0.8	0.7	0.6	0.4	0.3
Total	0.4	1.3	3.0	4.8	6.4	7.8	7.6	6.2	4.4	3.5

TABLE II: Expected and Observed Yields for background in the Fit Region

Base $ll\not{E}_T$ Selection

Category	WW	WZ	ZZ	$t\bar{t}$	DY	$W\gamma$	W+jets	Total	Data
$e\ e$	46.6	5.3	8.2	2.9	26.6	27.2	22.8	140 $\pm$12	144
$e\ \mu$	110.1	3.2	0.5	7.0	22.5	23.8	24.1	191 $\pm$17	191
$\mu\ \mu$	36.0	4.1	6.7	2.7	17.6	0.0	3.1	70 $\pm$ 6	58
e trk	37.8	2.6	3.3	2.6	10.3	6.5	10.9	74 $\pm$ 6	80
μ trk	20.6	1.6	2.3	1.5	5.3	1.1	5.8	38 $\pm$ 3	49
Total	251.0	16.9	20.9	16.8	82.2	58.5	66.6	513 $\pm$41	522

response. The Monte Carlo generator used for WW is MC@NLO [11], for WZ, ZZ, and $t\bar{t}$ it is PYTHIA [12], for $W\gamma$ it is the generator described in [13]. We use the CTEQ5L parton distribution functions (PDFs) to model the momentum distribution of the initial-state partons [14].

A correction of up to 10% per lepton is applied to the simulation based on measurements of the lepton reconstruction and identification efficiencies in data using Z decays. A further correction is applied to the $W\gamma$ background estimate using a measurement of the photon conversion veto efficiency in data. Trigger efficiencies are determined from $W \to e\nu$ data for electrons and from $Z \to \mu^+\mu^-$ data for muons.

The background from W+jets is estimated from a sample of events with an identified lepton and a jet that is required to pass loose isolation requirements and contain a track or energy cluster similar to those required in the lepton identification. The contribution of each event to the total yield is scaled by the probability that the jet is identified as a lepton. This probability is determined from multijet events collected with a set of jet-based triggers. A correction is applied for the small real lepton contribution using single W and Z boson Monte Carlo simulation.

VI. EVENT PROBABILITY CALCULATION

In order to separate the Higgs from other backgrounds we use an event-by-event calculation of the probability density $P_m(x_{obs})$ for a mode m which is either 10 different Higgs hypothesis, WW, ZZ, $W\gamma$ or Wparton:

$$P_m(x_{obs}) = \frac{1}{<\sigma_m>} \int \frac{d\sigma_m^{th}(y)}{dy} \epsilon(y) G(x_{obs}, y) dy \tag{1}$$

where

x_{obs}	are the observed "leptons" and $\vec{\not{E}}_T$,
y	are the true lepton four-vectors (include neutrinos),
σ_m^{th}	is leading-order theoretical calculation of the cross-section for mode m,
$\epsilon(y)$	is total event efficiency $\times$ acceptance
$G(x_{obs}, y)$	is an analytic model of resolution effects, and
$\frac{1}{<\sigma_m>}$	is the normalization.

The function $\epsilon(y)$ describes the probabilities of a parton level object (e, μ, γ or parton) to be reconstructed as the seven lepton categories. The efficiency function is purely from Monte Carlo for e or μ but a combination of Monte Carlo and data-driven measurements described in section V is applied for γ or parton. The event probability densities are used to construct a discriminant:

$$LR(x_{obs}) \equiv \frac{P_H(x_{obs})}{P_H(x_{obs}) + \Sigma_i k_i P_i(x_{obs})},$$

where H is one of the Higgs mass hypothesis, k_i is the expected fraction for each background and $\Sigma_i k_i = 1$. Figure 1 shows the likelihood ratio discriminator for $m_H = 160$ GeV/c^2. The dilepton pairs are categorized into two categories, highS/B and lowS/B, based on signal to background ratios. Because of the missing neutrinos in the final state, the integral in Equation 1 integrates out the unobserved degrees of freedom (DOF) reducing the 12 DOF in y to the eight measured DOF.

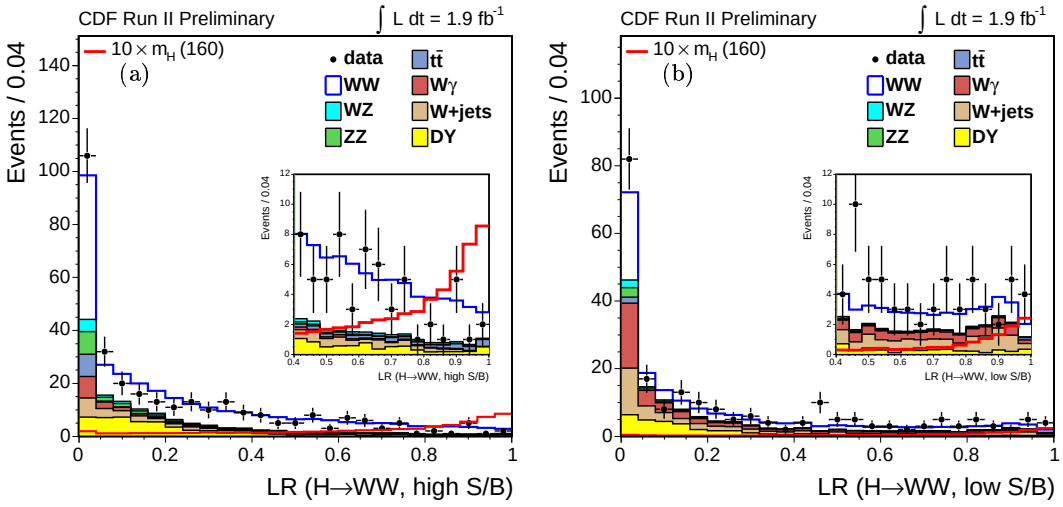

FIG. 1: Distribution of the $LR \equiv \frac{P_H}{P_H + \Sigma_i k_i P_i}$ Likelihood Ratio for (a) high S/B (b) low S/B for $m_H = 160$ GeV/c^2.

VII. SYSTEMATICS

Systematic uncertainties associated with the Monte Carlo simulation affect the Higgs, WW, WZ, ZZ, $W\gamma$, DY and $t\bar{t}$ simulations similarly. The uncertainties from the lepton selection and trigger efficiency measurements are propagated through the analysis, giving uncertainties of $1.1\% - 2.2\%$ and $0.3\% - 0.8\%$ for the respective efficiencies of the different signal and background processes. The uncertainties on the WW, $W\gamma$ and $t\bar{t}$ cross sections are assigned to be 10% [15], 10% [13], 5% [16] , and 15% [17, 18], respectively. For the $W\gamma$ background contribution, there is an additional uncertainty of 20% from the detector material description and conversion veto efficiency.

We assign an uncertainty due to higher order effects in WW a half of the difference between the leading-order (PYTHIA-based [12]) and next-to-leading order (MC@NLO [11]) acceptance. All the other processes are only simulated at leading-order and scaled by a k-factor to the NLO cross-sections. For these modes we assign the full difference observed in WW which is a 10% uncertainty. For Drell-Yan, which has been studied extensively at CDF and the simulation has been tuned to reproduce the kinematic distributions in data, we reduce this assignment to 5%. The detector acceptance variation due to PDF uncertainties is assessed to be 2% using the 20 pairs of PDF sets described in [19].

The systematic uncertainty on the W+jets background is determined from differences in the measured probability that a jet is identified as a lepton for jets collected using different jet E_T trigger thresholds. These variations correspond to changing the parton composition of the jets and the relative amount of contamination from real leptons.

The $\not\!\!E_T$ resolution modeling uncertainty is determined from comparisons of the data and the Monte Carlo simulation in a sample of dilepton events. For WW, WZ, $ZZ \to ll\nu\overline{\nu}$, and $t\bar{t}$ production, where it is an observed particle that produces the observed $\not\!\!E_T$, we determined the uncertainty to be 1%. The uncertainty due to the $\not\!\!E_T$ modeling for the Drell-Yan background is much larger (25%) than for other final states because it depends on the non-Gaussian tails of the resolution function. The individual contribution to the systematics are summarized in Table III.

The signal and background estimates obtained from simulation have an additional 6% uncertainty originating from the luminosity measurement [20].

TABLE III: Systematics. The additional 6% uncertainty due to luminosity measurement is not in the table.

	Fractional Uncertainty (%)							
	WW	WZ	ZZ	$t\bar{t}$	DY	$W\gamma$	W+jets	Higgs
$\not\!\!E_T$ Modeling	1.0	1.0	1.0	1.0	20.0	1.0	-	1.0
Conversions	-	-	-	-	-	20.0	-	-
NLO Acceptance	5.5	10.0	10.0	10.0	5.0	10.0	-	10.0
Cross-section	10.0	10.0	10.0	15.0	5.0	10.0	-	-
PDF Uncertainty	1.9	2.7	2.7	2.1	4.1	2.2	-	2.2
LepId $\pm 1\sigma$	1.5	1.4	1.3	1.5	1.5	1.2	-	1.5
Trigger Eff	2.1	2.1	2.1	2.0	3.4	7.0	-	3.3
Total	11.9	14.7	14.6	18.4	21.9	25.6	22.5	10.9

VIII. CROSS-CHECKS

In order to validate the data modeling, we use four control regions which test different aspects of the data modeling. The sample size of control regions are defined to be large enough to make statistically meaningful tests. The Drell-Yan region is the candidate selection without the $\not\!\!E_{T\text{spec}}$ and $\not\!\!E_{T,\text{sig}}$ requirements, so that a large number of the Drell-Yan event are accepted and is a high statistics tests of the acceptance, lepton id efficiency, and trigger efficiency calculations. The Base region selection with the opposite sign requirement reversed is called the same-sign region and tests the modeling of the jet and photons misidentified as leptons which dominate the region. To test the $\not\!\!E_T$ modeling we define two regions which are dominated by $\not\!\!E_T$-resolution tail of the Drell-Yan process. These are the Low-$\not\!\!E_{T\text{spec}}$ region which is the $ll\nu\overline{\nu}$ selection, but with $15 < \not\!\!E_{T\text{spec}} < 25$ GeV instead of $MET spec > 25$ GeV and the Low-$\not\!\!E_{T,\text{sig}}$ region which is $ll\nu\overline{\nu}$ selection with the $\not\!\!E_{T,\text{sig}}$ requirement reversed so that$\not\!\!E_{T,\text{sig}} < 2.5$ GeV$^{\frac{1}{2}}$. The yields in all four control regions are shown in Tables IV-VII.

TABLE IV: Expected and Observed Yields in the Drell-Yan Channel

Drell-Yan Control Region

Category	WW	WZ	ZZ	$t\bar{t}$	DY	$W\gamma$	W+jets	Total	Data
$e\ e$	4.6	25.9	32.2	0.9	69849.0	1.2	304.1	70200 ± 7700	67962
$e\ \mu$	4.4	0.1	0.0	0.8	54.9	0.3	14.8	75 ± 9	68
$\mu\ \mu$	4.3	21.7	28.6	0.9	56363.8	0.0	195.4	56600 ± 5100	54562
e trk	4.2	8.4	10.8	0.8	21609.8	0.4	320.1	22000 ± 3500	20307
μ trk	2.6	7.5	9.7	0.5	18830.1	0.0	174.5	19000 ± 1800	18081
Total	20.2	63.5	81.3	3.9	166707.6	1.9	1008.9	168000 ±18000	160980

TABLE V: Expected and Observed Yields in the Same-Sign Channel

Same-Sign $ll\not\!\!E_T$ Control Region

Category	WW	WZ	ZZ	$t\bar{t}$	DY	$W\gamma$	W+jets	Total	Data
$e\ e$	2.9	1.5	0.6	0.1	2.1	26.7	22.4	56 ± 8	59
$e\ \mu$	3.5	3.1	0.3	0.2	5.5	25.1	19.8	57 ± 8	71
$\mu\ \mu$	0.0	1.1	0.2	0.0	0.1	0.0	1.7	3 ± 1	4
e trk	1.2	1.1	0.2	0.1	1.1	6.4	6.3	16 ± 2	21
μ trk	0.0	0.6	0.1	0.0	0.3	1.1	3.1	5 ± 0	6
Total	7.6	7.3	1.3	0.4	9.1	59.3	53.4	138 ±19	161

IX. LIKELIHOOD RATIO TEST

Other than yield validation in control regions, we also validate the input variables for event probability calculation in Base region. Figure 2 shows the one dimensional distributions for each variable and χ^2 and Kolmogorov-Smirnov(KS) Tests are both presented.

In analogy to the likelihood ratio discriminator variable we use for separating Higgs events from background, we can define discriminants for each of the background hypotheses. Figure 3 shows the distributions of these LR variables for the three dominant background distributions with the data overlayed. The overall agreement between data and

TABLE VI: Expected and Observed Yields in the Low-$\not\!\!E_{T\,\mathrm{spec}}$ Channel

Low $\not\!\!E_T$, High $\not\!\!E_{T\,\mathrm{spec}}$ Control Region

Category	WW	WZ	ZZ	$t\bar{t}$	DY	$W\gamma$	W+jets	Total	Data
e e	3.7	1.0	1.0	0.4	33.7	2.4	4.6	47 ± 7	40
e μ	6.0	0.3	0.1	0.5	31.0	1.7	3.4	43 ± 7	31
μ μ	2.8	0.7	0.8	0.4	28.5	0.0	0.9	34 ± 6	33
e trk	3.1	0.5	0.4	0.3	35.4	0.5	2.9	43 ± 8	38
μ trk	1.8	0.3	0.3	0.2	7.8	0.1	1.0	11 ± 2	9
Total	17.4	2.6	2.7	1.8	136.5	4.7	12.8	179 ±30	151

TABLE VII: Expected and Observed Yields in the Low-$\not\!\!E_{T,\mathrm{sig}}$ Channel

High $\not\!\!E_T$, Low $\not\!\!E_{T,\mathrm{sig}}$ Control Region

Category	WW	WZ	ZZ	$t\bar{t}$	DY	$W\gamma$	W+jets	Total	Data
e e	2.9	0.5	0.5	0.2	17.8	2.4	3.4	28 ±4	26
e μ	0.0	0.0	0.0	0.0	0.0	0.0	0.0	0 ±0	0
μ μ	2.3	0.4	0.5	0.2	10.6	0.0	0.5	14 ±2	13
e trk	2.5	0.2	0.2	0.2	6.5	0.6	1.0	11 ±1	11
μ trk	1.4	0.1	0.2	0.1	3.8	0.1	0.6	6 ±1	5
Total	9.1	1.3	1.4	0.8	38.7	3.1	5.4	60 ±9	55

expectations gives us confidence that the background models accurately describe the distribution of the data across phase space.

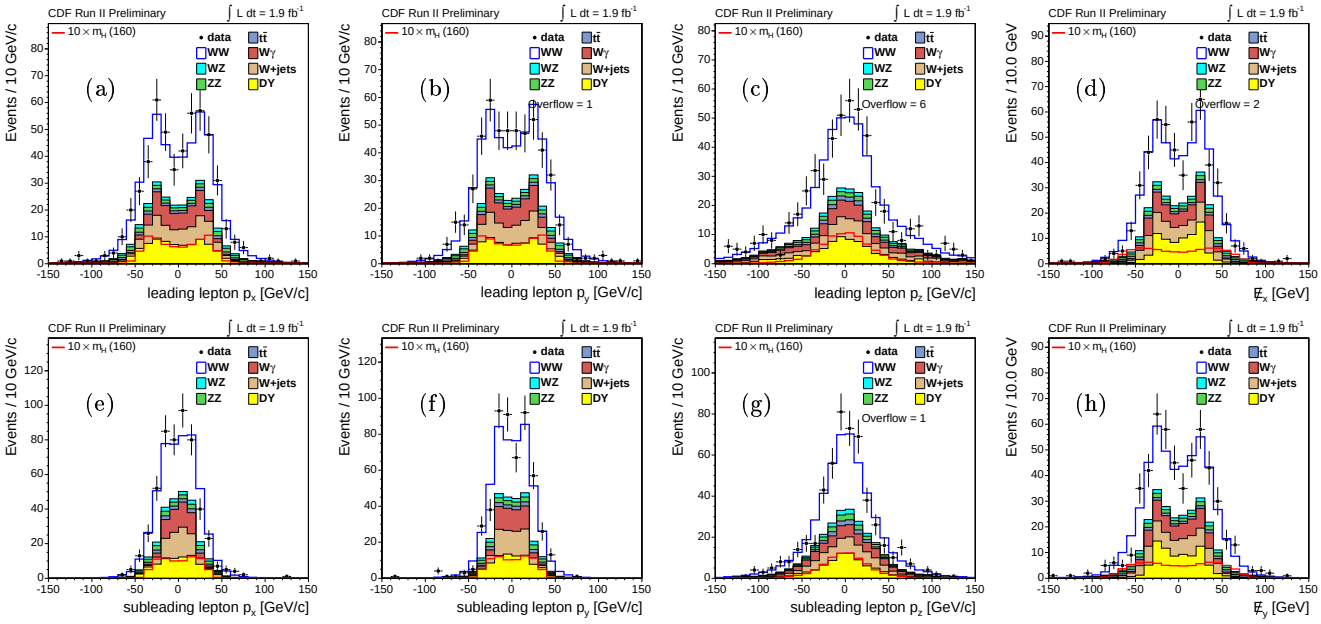

FIG. 2: Distribution of input variables for Event Probability Calculation (a) leading lepton p_x (b) leading lepton p_y (c) leading lepton p_z (d) $\not\!\!E_{T\,x}$ (e) subleading lepton p_x (f) subleading lepton p_y (g) subleading lepton p_z (h) $\not\!\!E_{T\,y}$

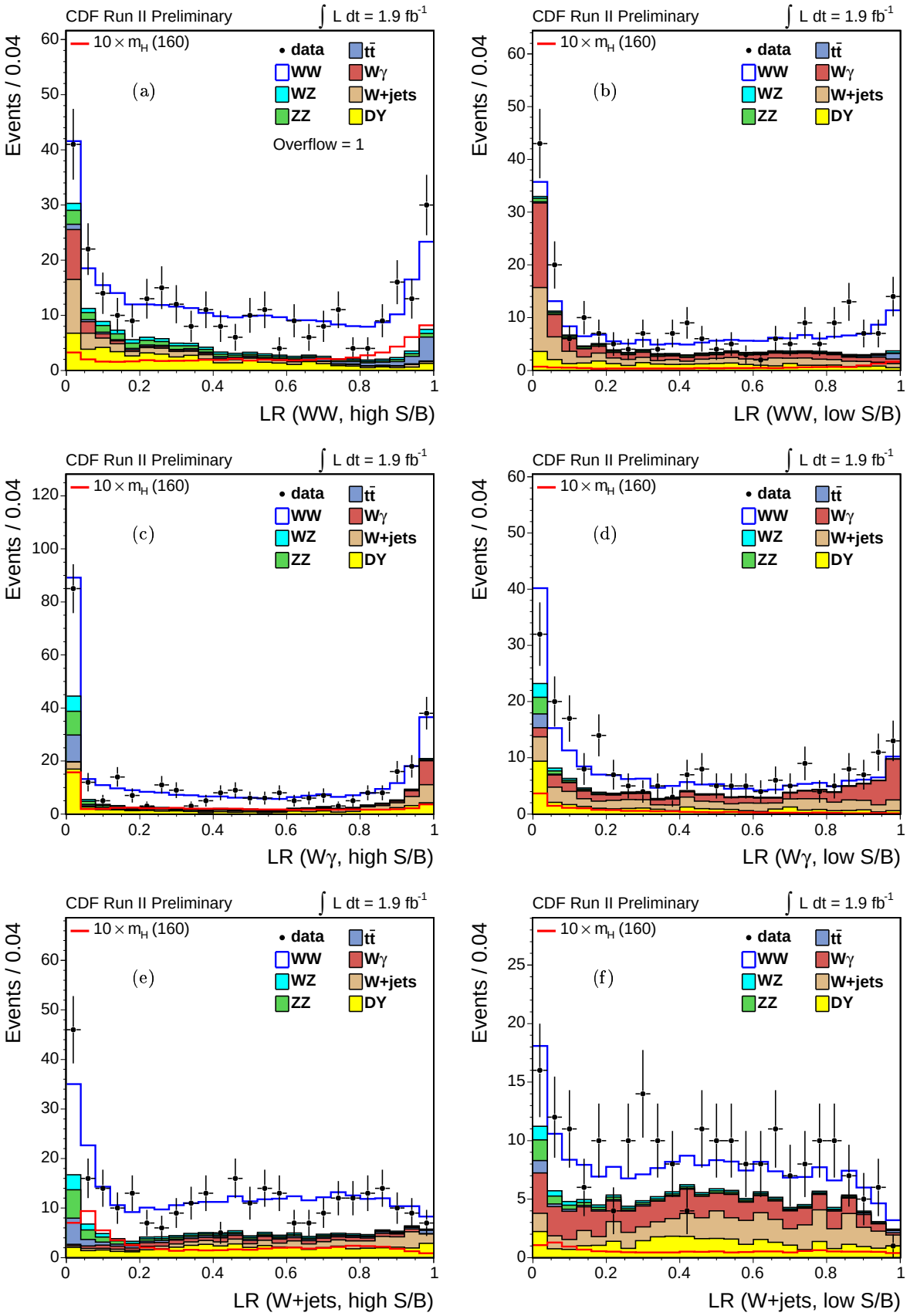

FIG. 3: The likelihood ratio distribution of (a)(b) $LR \equiv \frac{P_{WW}}{P_{WW}+\Sigma_i k_i P_i}$ (c)(d) $LR \equiv \frac{P_{W\gamma}}{P_{W\gamma}+\Sigma_i k_i P_i}$ (e)(f) $LR \equiv \frac{P_{Wparton}}{P_{Wparton}+\Sigma_i k_i P_i}$ for high S/B and low S/B channel, respectively.

$M\_H(GeV/c^2)$	110	120	130	140	150	160	170	180	190	200
$\sigma_{SM}(HWW)(pb)$	0.057	0.134	0.230	0.312	0.358	0.388	0.344	0.278	0.194	0.155
$median(pb)$	3.9	2.9	2.4	2.2	1.8	1.2	1.1	1.3	1.4	1.5
$Observed(pb)$	4.8	2.8	1.6	1.5	1.1	0.8	0.8	0.8	1.4	1.9
$+2\sigma/\sigma_{SM}$	139.4	45.1	21.0	13.7	10.4	6.1	6.5	9.1	13.7	19.5
$+1\sigma/\sigma_{SM}$	96.4	31.7	15.2	9.6	7.3	4.4	4.5	6.5	10.2	14.1
$median/\sigma_{SM}$	69.0	21.7	10.7	6.9	5.2	3.1	3.2	4.6	7.1	9.7
$-1\sigma/sigma_{SM}$	48.9	15.4	7.7	5.0	3.7	2.2	2.3	3.2	5.0	6.9
$-2\sigma/\sigma_{SM}$	35.9	11.2	5.8	3.8	2.9	1.6	1.7	2.4	3.8	5.2
$Observed/\sigma_{SM}$	83.0	20.9	7.0	4.7	3.2	2.0	2.4	3.0	7.0	11.6

TABLE VIII: Expected and Observed Limit for Higgs at 1.9 fb^{-1} with Systematics (the ratios include the uncertainty on σ_{SM}).

X. RESULTS

In order to determine the cross-section and sensitivity of the Higgs signal, we perform a binned maximum likelihood fit over likelihood ratio discriminator. All the signals and backgrounds are allowed to float in the fit, but the ratio of signals in the two channels and all of the backgrounds are constrained to their expectations with a set Gaussian constraints which implement all of the assumed correlations between the systematics uncertainties. The total signal yield is allowed to float.

The 95% CL limit is determined with a set of 1000 Monte Carlo background-only experiments based on the expected yields varied by the assigned systematics. Again the correlations between the systematics for different backgrounds are included. For each experiment a test statistic is formed from the difference in the likelihood value with the background-only model and with the signal yield at the best fit value. The observed 95% C.L. limit for $m_H = 160$ GeV/c^2 is 0.8 pb which is 2.0 times the Standard Model prediction at NNLL level[3] while the median of expected limit is $3.1^{+1.3}_{-0.9}$.

XI. SUMMARY

We have searched for Standard Model Higgs decay to WW^* in the $ll\nu\nu$ final state using the Matrix Element methods. The observed 95% C.L. limit compares well with the expected limit as shown in Table VIII, as well as Figure 4. We see no sign of a significant excess or deficit at any Higgs mass.

[1] The LEP Electroweak Working Group, http://lepewwg.web.cern.ch/LEPEWWG/.
[2] M. Spira (1998), hep-ph/9810289.
[3] S. Catani, D. de Florian, M. Grazzini, and P. Nason, JHEP **07**, 028 (2003), hep-ph/0306211.
[4] J. Campbell and K. Ellis, MCFM - Monte Carlo for FeMtobarn processes, http://mcfm.fnal.gov/.
[5] R. Blair, *et al.* (CDF Collaboration) (1996), FERMILAB-PUB-96/390-E.
[6] A. Sill *et al.*, Nucl. Instrum. Methods A **447**, 1 (2000).
[7] A. Affolder *et al.*, Nucl. Instrum. Methods A **453**, 84 (2000).
[8] T. Affolder *et al.*, Nucl. Instrum. Methods A **526**, 249 (2004).

[9] K. Hagiwara, S. Ishihara, R. Szalapski, and D. Zeppenfeld, Phys. Rev. D **48**, 2182 (1993).
[10] R. Brun, R. Hagelberg, M. Hansroul, and J. Lassalle, CERN-DD-78-2-REV and CERN-DD-78-2.
[11] S. Frixione and B. R. Webber, JHEP **06**, 029 (2002), hep-ph/0204244.
[12] T. Sjostrand, S. Mrenna, and P. Skands, JHEP **05**, 026 (2006).
[13] U. Baur and E. L. Berger, Phys. Rev. **D47**, 4889 (1993).
[14] H. L. Lai *et al.* (CTEQ), Eur. Phys. J. **C12**, 375 (2000).
[15] J. M. Campbell and R. K. Ellis, Phys. Rev. **D60**, 113006 (1999).
[16] A. Abulencia et al. (CDF) (2005), hep-ex/0508029.
[17] N. Kidonakis and R. Vogt, Phys. Rev. **D68**, 114014 (2003).
[18] M. Cacciari, S. Frixione, M. L. Mangano, P. Nason, and G. Ridolfi, JHEP **04**, 068 (2004).
[19] S. Kretzer, H. L. Lai, F. I. Olness, and W. K. Tung, Phys. Rev. **D69**, 114005 (2004).
[20] D. Acosta *et al.*, Nucl. Instrum. Meth. **A494**, 57 (2002).

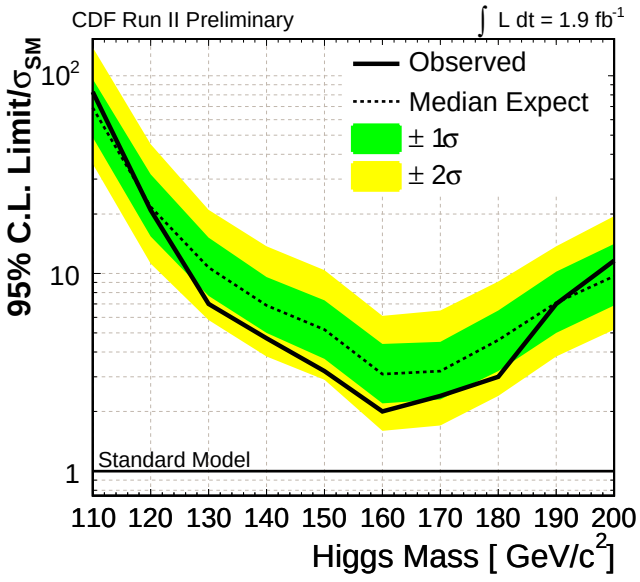

FIG. 4: The ratio of 95% C.L.production cross section limit to Standard Model calculation in NNLL level for 10 different Higgs mass.